

Mineralogy and chronology of the young mare volcanism in the Procellarum-KREEP-Terrane

Received: 28 December 2021

Accepted: 11 November 2022

Published online: 12 January 2023

 Check for updates

Yuqi Qian^{1,8}, Zhenbing She^{2,8}, Qi He^{1,8}, Long Xiao¹✉, Zaicong Wang¹✉, James W. Head³, Lingzhi Sun⁴, Yiran Wang⁵, Bo Wu⁵, Xiang Wu¹, Biji Luo¹, Kenan Cao², Yiheng Li¹, Mingtan Dong², Wenlei Song⁶, Fabin Pan¹, Joseph Michalski⁷, Binlong Ye⁷, Jiawei Zhao¹, Siyuan Zhao¹, Jun Huang¹, Jiannan Zhao¹, Jiang Wang¹, Keqing Zong¹ & Zhaochu Hu¹

Young lunar mare basalts are recent volcanic products distributed mainly in the Procellarum-KREEP-Terrane. However, these young basalts were never investigated in situ until 2013 by Chang'e-3, and then sampled by Chang'e-5 in 2020. Using the returned Chang'e-5 samples as ground truth, and examining Moon Mineralogy Mapper data globally, we found the young basalts containing less abundant olivine (<10%) than previously suggested. The Chang'e-3 and Chang'e-5 basalts belong to a type of underrepresented basalt. We reassessed the model ages of the young basalts using the new chronology function calibrated by the Chang'e-5 samples and found the young basalts have a trend of increasing TiO₂ abundance with time. The young basalts with an age of around 2.0 Ga (billion years ago) are widespread in the Procellarum-KREEP-Terrane, including the Chang'e-5 unit. This indicates mare volcanism was still active at that time and an additional heat source or mechanism may be needed compared to older basalts. Young mare samples from Chang'e-5 and other potential sites are needed to constrain the late lunar thermal and volcanic history.

The young mare basalts are the products of recent lunar volcanism, with low to intermediate titanium (>4%) and high iron abundance (>20%)¹. They are mainly distributed in the centre of the Procellarum-KREEP-Terrane² (PKT, Fig. 1a), where volcanic activity may be extended by elevated heat-producing elements and volcanism was active until 1.2 Ga (billion years ago)³.

To understand the nature and evolution of young lunar volcanic rocks, determining their mineralogy and chronology is crucial. The young basalts were first proposed to be rich in iron-bearing glass or olivine on the basis of telescopic observation of their strong and broad 1 μm spectral feature⁴. Subsequent orbital data^{1,5–7} confirmed the broad 1 μm and the weak 2 μm spectral absorptions of these western-nearside

¹State Key Laboratory of Geological Processes and Mineral Resources, Planetary Science Institute, School of Earth Sciences, China University of Geosciences, Wuhan, China. ²State Key Laboratory of Biogeology and Environmental Geology, School of Earth Sciences, China University of Geosciences, Wuhan, China. ³Department of Earth, Environmental and Planetary Sciences, Brown University, Providence, RI, USA. ⁴Department of Earth Sciences, Hawaii Institute of Geophysics and Planetology, University of Hawaii at Manoa, Honolulu, HI, USA. ⁵Planetary Remote Sensing Laboratory, Department of Land Surveying and Geo-Informatics, The Hong Kong Polytechnic University, Hong Kong, China. ⁶State Key Laboratory of Continental Dynamics, Department of Geology, Northwest University, Xi'an, China. ⁷Department of Earth Sciences and Laboratory for Space Research, University of Hong Kong, Hong Kong, China. ⁸These authors contributed equally: Yuqi Qian, Zhenbing She, Qi He. ✉e-mail: longxiao@cug.edu.cn; zaicongwang@cug.edu.cn;

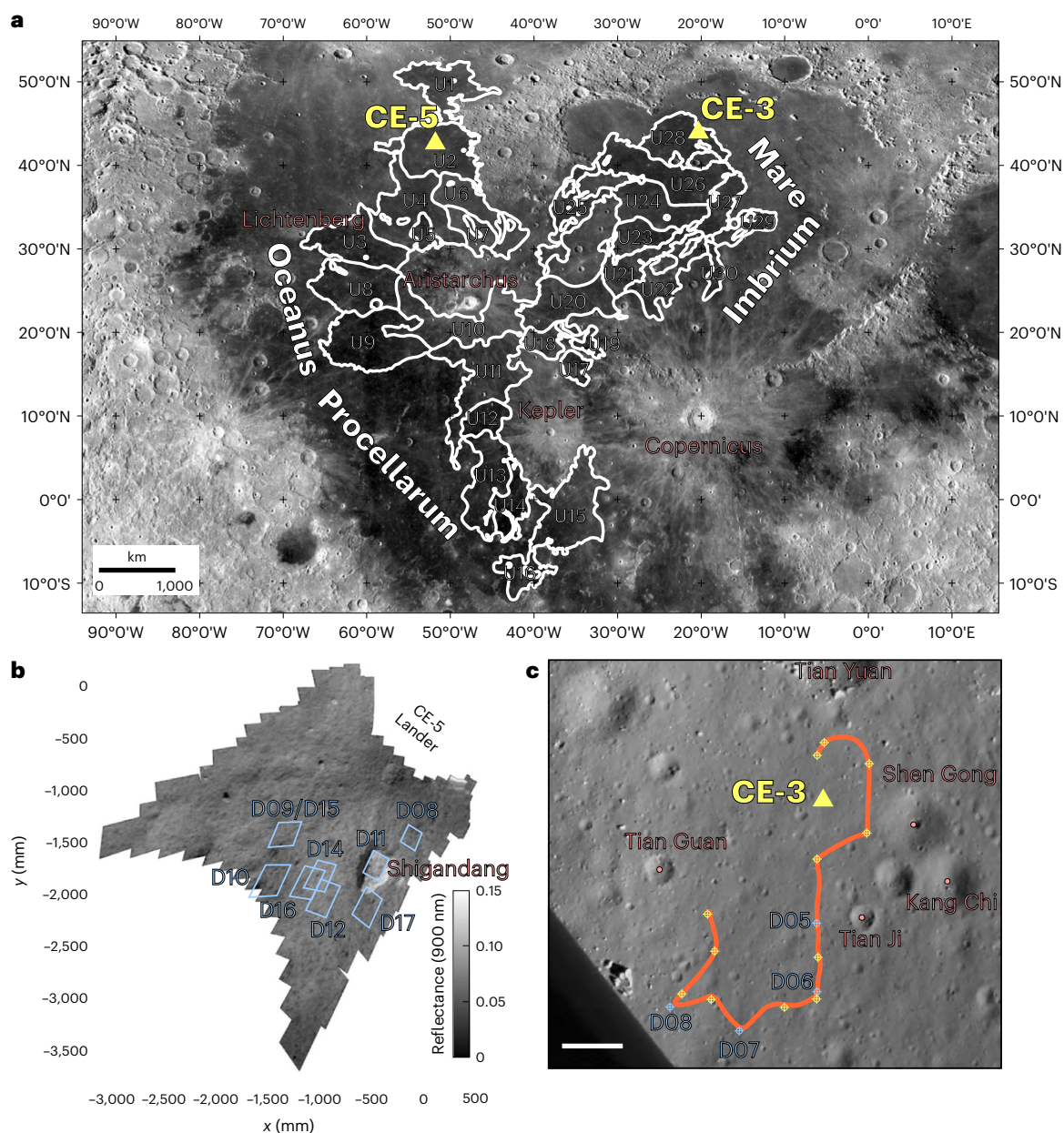


Fig. 1 | In situ investigation locations of the CE-3 and CE-5 missions. **a**, Locations of the CE-3 and CE-5 landing sites (yellow triangles). The white lines indicate the boundary of the young mare basalts (U1 to U30). The basemap is a LROC WAC image (NASA/GSFC/ASU). **b**, Locations of each CE-5 LMS measurement (D08, D09, D10, D11, D12, D14, D15, D16, D17). The coordinates are

relative to the centre of LMS. The basemap is LMS all views scan mode data at 900 nm. **c**, Locations of each CE-3 VNIS and APXS measurement (D05, D06, D07, D08; blue crosses). The red path represents the rover moving path and the yellow crosses represent the stopping sites. The basemap is a landing camera image. The red names in each panel identify the main features of the area. Scale bar, 10 m.

young basalts. This asymmetric $1\ \mu\text{m}$ feature was interpreted to be due to olivine enrichment^{1,5-7}, which is roughly $50 \pm 10\%$ by volume as determined by Clementine multispectral data⁸. In addition, the olivine abundance of these young units varies stratigraphically, with younger flows tending to have higher abundances^{5,6}. The mare basalts around Lichtenberg crater (Fig. 1a) have the strongest olivine signatures⁶, decreasing progressively to the older southern units.

These young basalts have not been visited by previous missions⁹. Thus, our understanding relied solely on remote sensing techniques^{1,4-7}, which lack ground truth verification. Recently, young basalts were first investigated in situ by Chang'e-3 (CE-3) in 2013, and then sampled by Chang'e-5 (CE-5) in 2020. CE-3, with the Yutu rover, landed at 19.51°W , 44.12°N in northwestern Mare Imbrium (Fig. 1a) on an Eratosthenian-aged mare unit¹⁰. CE-5, the first lunar sample-return

mission of China¹¹, collected 1,731 g of lunar samples from northern Oceanus Procellarum at 51.92°W , 43.06°N (Fig. 1a). CE-5 landed on an Eratosthenian-aged mare unit, named Em4 (ref. 12) (the fourth Eratosthenian-aged mare unit in the region; Extended Data Fig. 1c,d), with a Pb–Pb isochron age of $2.0\ \text{Ga}$ ^{13,14}. Both the CE-3 and CE-5 sites are located in the young mare basalts, providing an opportunity to study the young lunar volcanism.

The CE-3 Yutu rover carried a visible and near-infrared imaging spectrometer (VNIS) (450–2,400 nm) and an active particle-induced X-ray spectrometer (APXS)¹⁵; the CE-5 lander carried a lunar mineralogical spectrometer (LMS) (480–3,200 nm)¹¹. The CE-3 VNIS and APXS and CE-5 LMS in situ data (Fig. 1b,c) together with the CE-5 samples can be used as solid ground truth for calibrating the orbital measurements of the young basalts. The laboratory Raman spectroscopy,

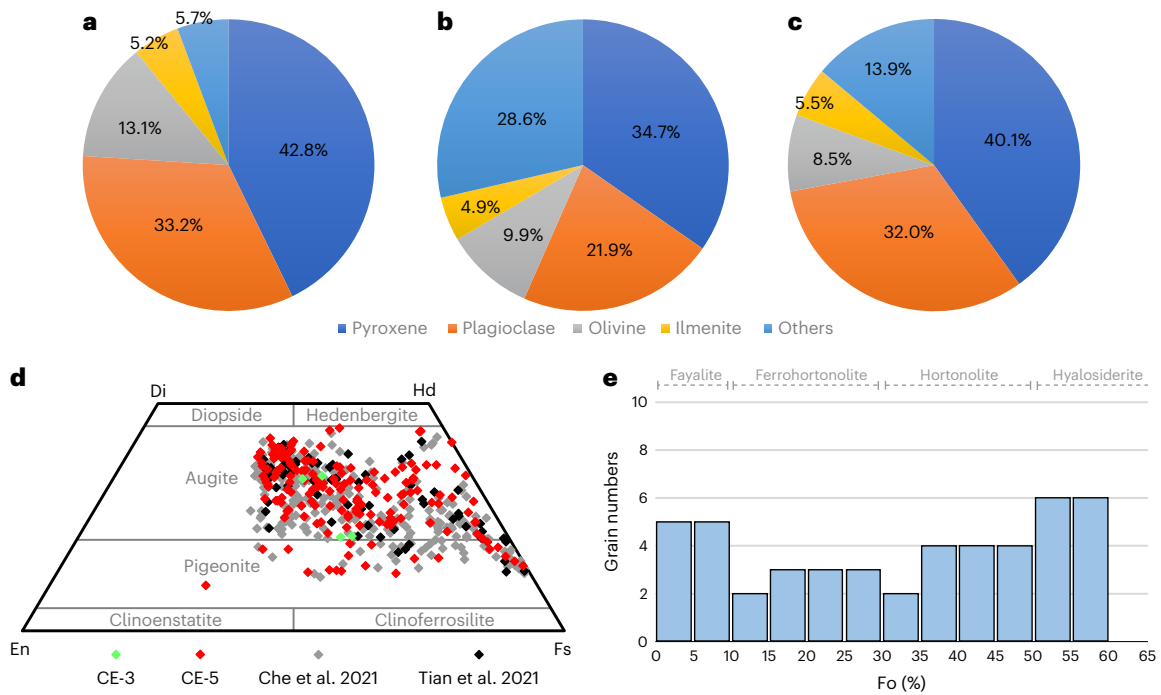


Fig. 2 | Mineral abundance and composition of the CE-5 sample. a, Mineral abundance of CE5C0400 based on Raman spectroscopy. **b,** Mineral abundance of CE5C0400 based on TIMA EDS analysis. **c,** Mineral abundance of the CE-5 sample

summarized in Supplementary Table 1. **d,** Pyroxene type of the CE-5 regolith based on electron probe analysis. **e,** Olivine type of the CE-5 regolith based on electron probe analysis.

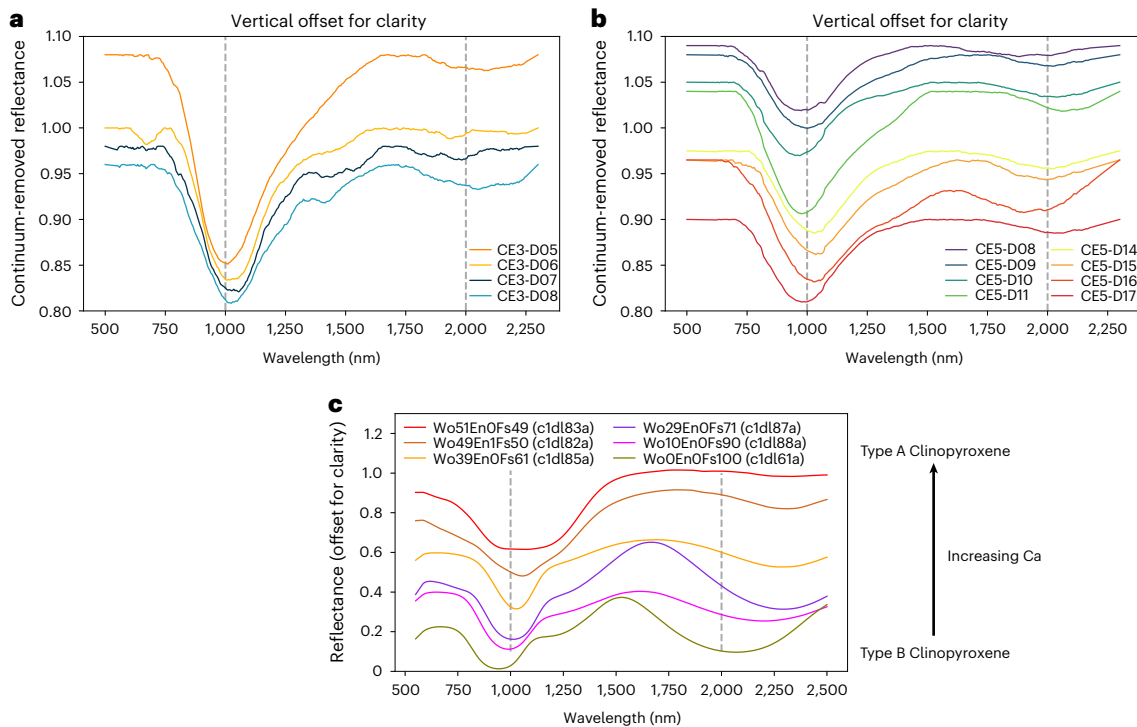


Fig. 3 | Continuum-removed reflectance obtained by CE-3 and CE-5 on the lunar surface. a, Each line represents a continuum-removed spectrum of the CE-3 VNIS from northwestern Mare Imbrium. **b,** Each line represents a continuum-removed spectrum of the CE-5 LMS from northern Oceanus

Procellarum. **c,** Relation between clinopyroxene spectra and calcium content²⁴. With increasing calcium content, the band I absorption becomes broader and band II becomes shallower. Each line represents a RELAB spectrum.

energy dispersive spectrometer (EDS) analysis and electron probe measurements were thus used to analyse the mineral abundance and composition of the CE-5 samples.

To constrain the mineralogy and chronology of the young mare basalts on the Moon, the lookup table technique¹⁶ was further used to unmix the spectra obtained by the Moon Mineralogical Mapper

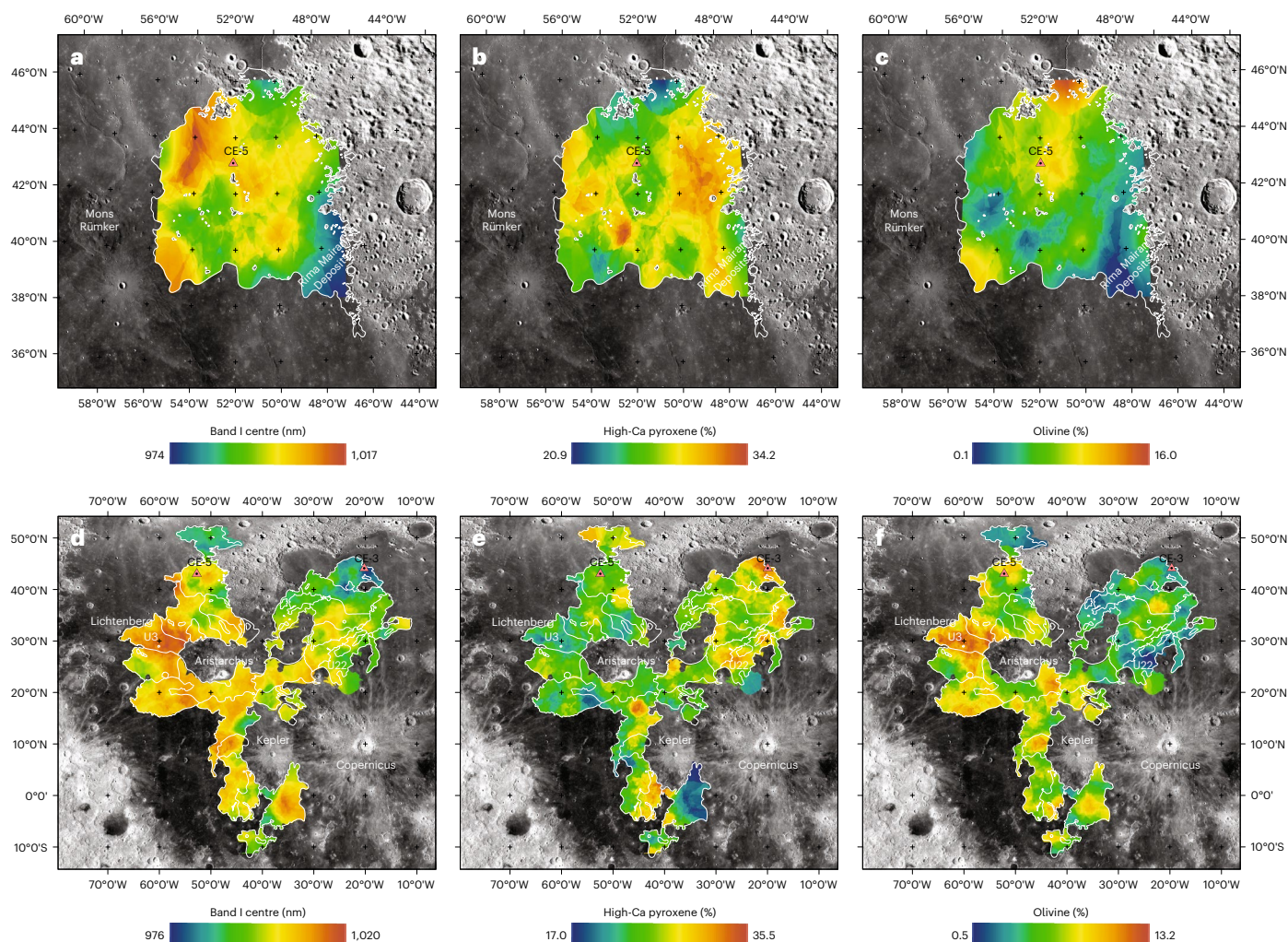


Fig. 4 | Mineralogy of Em4 and the young mare basalts. a–c, Band I centre position (a), high-Ca pyroxene abundance (b) and olivine abundance (c) of Em4. **d–f,** Band I centre position (d), high-Ca pyroxene abundance (e) and olivine abundance (f) of the young mare basalts. CE-5 landed on the Em4 unit. The basemap is a LROC WAC image (NASA/GSFC/ASU).

(M³) (430–3,000 nm)¹⁷ on the basis of the ground truth from CE-3 and CE-5. In addition, the lunar chronology function has been calibrated by the CE-5 basalt age (2.0 Ga)^{13,14} in the less constrained range of the function between 1.0 and 3.0 Ga^{18,19}. The new chronology function is a significant step in updating the ages of the young basalts because all of their ages are within 1.0–3.0 Ga³. The geological boundaries of the young basalts were delineated on the basis of Lunar Reconnaissance Orbiter Camera (LROC) Wide Angle Camera (WAC) albedo and Clementine ultraviolet-visible light (UV-vis) false colour maps (Fig. 1 and Extended Data Fig. 1a,b) and labelled from U1 to U30. Using the new chronology function, the crater size-frequency distribution (CSFD) measurements were used to obtain the model ages of all 30 mapped young mare units. Together, the mineralogy and chronology of the young basalts provides important implications for the petrology and evolution of the young lunar volcanism.

Results

CE-5 sample mineralogy

The mineralogy of 4,830 particles with size smaller than 45 μm from the CE-5 scooped sample CE5C0400 was first determined by Raman spectral analysis on the basis of the characteristic peaks of typical lunar minerals (Supplementary Data 2). Then, the modal abundance of key minerals was estimated on the basis of their spherical equivalent volume: pyroxene (42.8%), plagioclase (33.2%), olivine (13.1%),

Fe-Ti oxide (5.2%, mainly ilmenite), glass (3.4%) and minor phases (for example, quartz and apatite; roughly 2.3%) (Fig. 2a). For larger particles (50–300 μm, 612 grains), the TESCAN Integrated Mineral Analyzer (TIMA) EDS analysis was used to determine their mineralogy. Additional phases were distinguished by this method, including augite, pigeonite, glass, plagioclase, olivine, quartz, K-glass, K-feldspar and so on, but no orthopyroxene was found. Mineral abundances by area are shown in Fig. 2b: pyroxene (34.7%), glass (25.7%), plagioclase (21.9%), olivine (9.9%), ilmenite (4.9%) and minor phases (2.9%).

In addition, the mineralogy of the CE-5 samples from other studies were summarized together (Supplementary Table 1)^{13,20,21}. Combining the results from all studies yields an olivine abundance of $8.5 \pm 2.6\%$ (Fig. 2c), far smaller than previously reported of the young basalts^{5,8}. Combining the datasets from multiple techniques and variable fractions for samples helps address the issue of heterogeneity and representative sampling when working with small masses.

The mineral composition of pyroxene (164 grains) and olivine (47 grains) for CE5C0400 was determined by an electron microprobe analyser (EMPA). Augite is the dominant pyroxene type (76.8%), followed by pigeonite (23.2%), and no orthopyroxene was found (Fig. 2c). The average composition of pyroxene is $Wo_{30.5}En_{25.2}Fs_{44.3}$. Our pyroxene composition matches well with the results of other aliquots of CE-5 samples (grey and black diamonds, Fig. 2d)^{13,20}. The Fo value of olivine is between 0 and 60 (mean Fo, 31.9; Fig. 2e). Most of the olivines (74.5%)

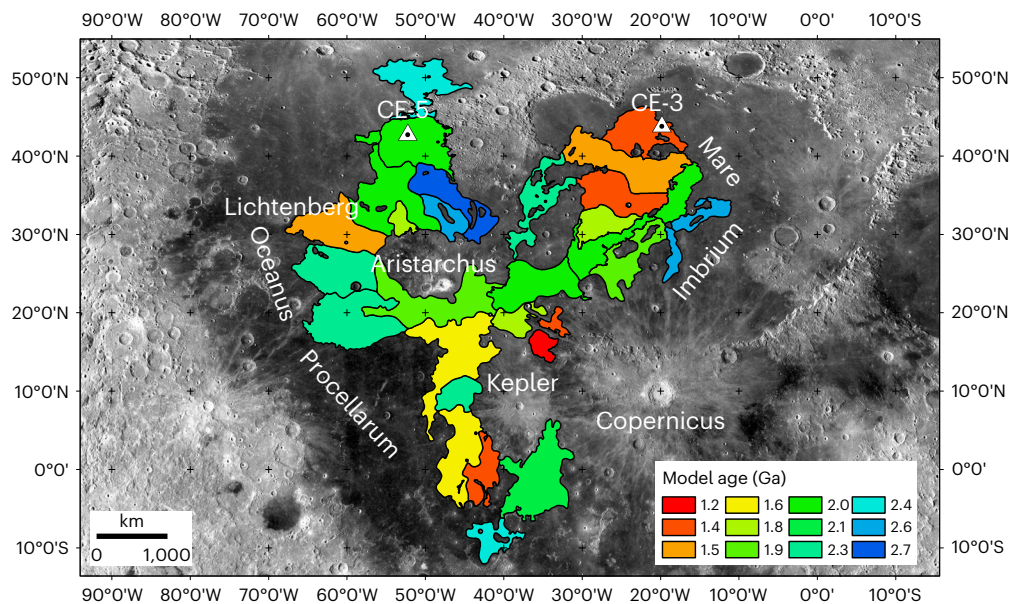


Fig. 5 | Model ages of the young mare basalts determined through CSFD measurements using the new lunar chronology function. White triangles represent the CE-3 and CE-5 landing sites.

are iron-rich with Fo smaller than 50, in contrast to the previously reported numbers (Fo > 50) by remote sensing^{5,20,22}.

CE-3 VNIS and CE-5 LMS mineralogy

CE-5 LMS acquired 11 spectra around the lander in all-band detection mode (Fig. 1b), and eight of them were used. All seven measurements of the regolith show a deep and broad 1 μm and a weak 2 μm absorption (Fig. 3b), consistent with spectral features^{5–7} of the young basalts observed by M³. The band I centre wavelength is slightly shorter than 1 μm for CE5-D08, CE5-D10 and CE5-D17, and slightly longer than 1 μm for CE5-D09, CE5-D14, CE5-D15 and CE5-D16. The broad 1 μm band was previously interpreted to be due to abundant olivine^{1,4–8}. However, the laboratory results of the CE-5 samples show that the olivine abundance is lower than 10% at the CE-5 site (Fig. 2c). Therefore, the broad 1 μm feature is more likely to be due to the special composition of pyroxene (Fig. 2d). Clinopyroxene has two spectral types, that is, type A and type B²³. Type B clinopyroxene has both a narrow symmetrical band I and a broad band II caused by Fe²⁺ in the M2 site; type A clinopyroxene only has a complex band I near 1 μm caused by Fe²⁺ in the M1 site²³. Type A clinopyroxene tends to have higher calcium content²⁴ (Fig. 3c). Of the pyroxene investigated by EMPA, 56.7% has Wo > 30, which belongs to an intermediate type closer to type A and could explain the observed relatively broad 1 μm and weak 2 μm absorptions. In addition, the ideal site allocation of cations at T, M1 and M2 were calculated on the basis of EMPA data²⁵; according to which, 49.2% of Fe²⁺ is sited at the M1 site, supporting an intermediate spectral nature.

The LMS spectral measurement on Shigandang Rock (CE5-D11) has a deep and broad 1 μm absorption and a weak 2 μm absorption (Fig. 3b), similar to the regolith measurements but with deeper absorptions. The Shigandang Rock is likely to represent the bedrock and the surrounding regolith is the products of its comminution.

The CE-3 VNIS acquired four spectra during the Yutu rover traverse (Fig. 1c). All of them have a broad 1 μm absorption and a weak 2 μm absorption, similar to CE-5, including CE-3-D06 and CE-3-D08 that were proposed to contain mainly olivine²⁶. However, on the basis of APXS data using mixture modelling of the chemical composition²⁷, the CE-3 site has an olivine abundance of only 13.8 \pm 5.7% with augite, pigeonite and ilmenite abundance of 35.0, 16.5 and 8.2 wt%, respectively.

M³ mineralogy

The olivine abundance in the two locations of the young basalts, the CE-3 (13.8 \pm 5.7%) and CE-5 (8.5 \pm 2.6%) sites, deviates significantly from previous studies (50 \pm 10%)^{1,4–8}, which calls into question the mineralogy of other locations. Some previous studies focus only on the band I absorption, which makes spectral descriptions incomplete^{5,6}. Furthermore, the young mare basalts may be more evolved than all previous mare samples, on the basis of the analysis of CE-3 (Mg# of 38) and CE-5 (Mg# of 34) samples with abnormally low Mg#^{13,21,27}. These factors suggest that previous interpretations of the mineralogy of young basalts based on remote sensing alone may be inaccurate. To address these issues and extend our research laterally, we used the lookup table technique following the routine of Sun et al.¹⁶, which can be applied to variable Mg# values. For Em4 and the other young mare units, the bulk mineralogy of 200 and 1,741 small fresh craters was calculated from thermally corrected M³ spectra²⁸ and then interpolated using the Kriging method to produce mineral distribution maps (Fig. 4 and Extended Data Fig. 2). The band I and II centre positions were also computed because they are sensitive to the key minerals of interest (Fig. 4a,d and Extended Data Fig. 2a,d).

The Em4 unit on which CE-5 landed (U2; Extended Data Fig. 1a,b) has average band I and II centre positions at 996 and 2,066 nm based on M³ data, respectively. Both the M³ band I and II centre positions are close to the in situ LMS measurements (Fig. 3b), indicating the CE-5 in situ spectra could be representative of the entire unit.

The CE-5 site has M³ mineral abundances of high-Ca pyroxene (28 \pm 1.0%), low-Ca pyroxene (10 \pm 1.1%), olivine (10 \pm 0.8%) and plagioclase (53 \pm 2.7%). This reinterpreted olivine abundance agrees well with olivine abundances of the samples (8.5 \pm 2.6%). The consistent results indicate that the lookup table technique is reliable and strengthens the interpretation that olivine is not as abundant as previously interpreted^{1,4–7}. There are some internal mineralogical variations inside Em4. The southeast corner of Em4 has shorter band I and band II centre wavelengths, lower olivine and plagioclase abundances, but higher low-Ca pyroxene abundance (Fig. 4a–c and Extended Data Fig. 2a–c). We interpret the difference in mineralogy in the southeast corner of Em4 to be due to an independent younger eruption²⁹. Rima Sharp, whose source is to the north in Sinus Roris, erupted first at 2.0 Ga^{13,14} and its lava covered the current Em4 area. Rima Mairan erupted later

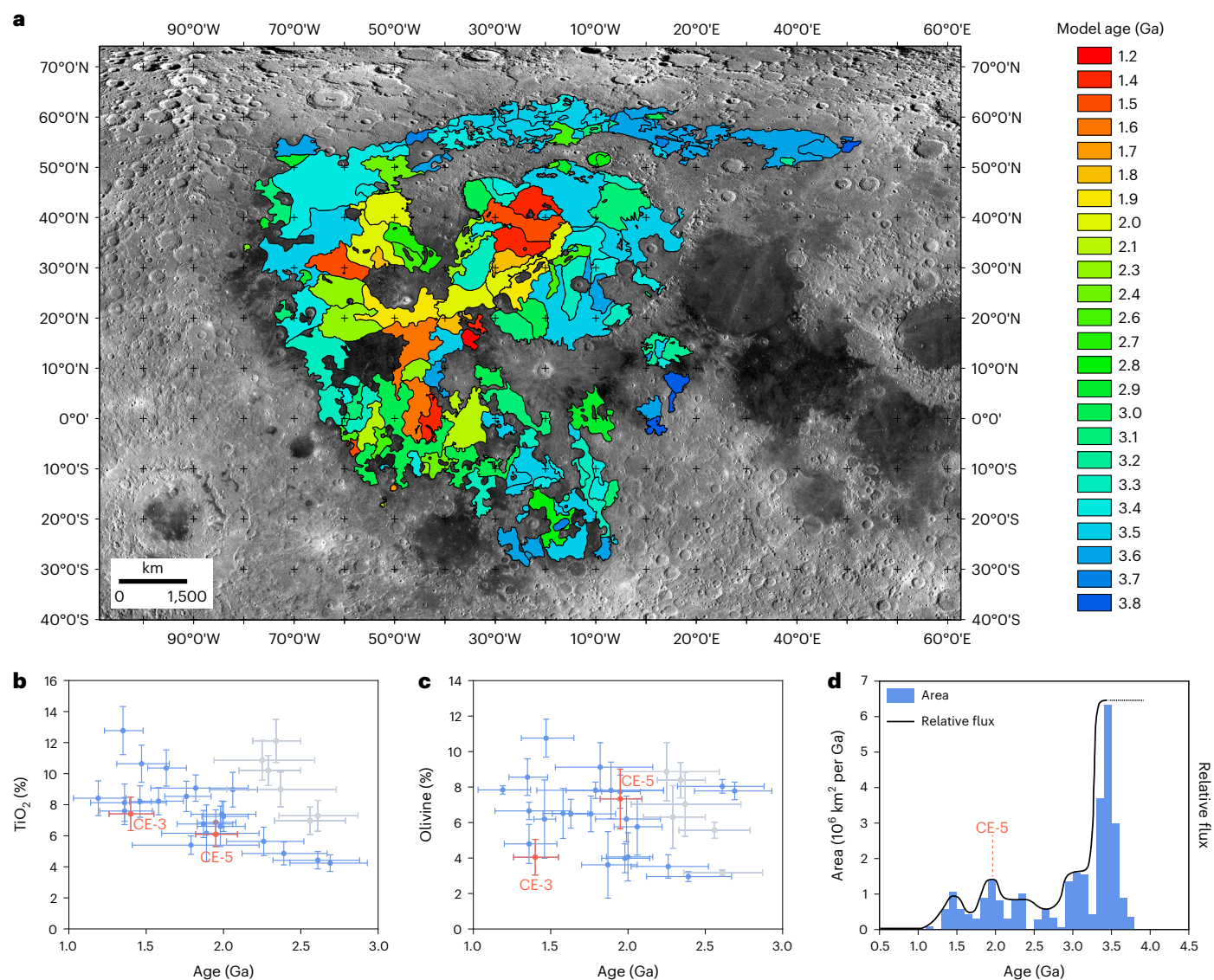


Fig. 6 | Age and composition of mare basalts in the PKT. a, Model ages of mare basalts in PKT. The age of young basalts was determined in this study. The age of other basalts was determined by Hiesinger et al.³. **b, c**, The relation between TiO₂ (**a**) and olivine (**b**) abundances and the age of young mare basalts (blue points, CE-3 and CE-5 basalts are highlighted by red colour), if excluded U8, U9, U12, U16,

U29 and U30 (grey points). The centre of each point in the y direction represents the mean value of composition in terms of area, and error bars represent the s.d.; the centre of each point in the x direction represents the age and uncertainties from CSFD measurements. **d**, Relative eruption flux of the mare volcanism in PKT.

at 1.4 Ga²⁹. Lavas from Rima Mairan are deposited in the southeast of Em4 with slightly lower olivine abundance.

Overall, the entire area of young basalts has average band I and II centre positions at 1,001 and 2,035 nm (Fig. 4d and Extended Data Fig. 2d), respectively. The average mineral abundances are high-Ca pyroxene (25 ± 1.0%), low-Ca pyroxene (19 ± 1.1%), olivine (6 ± 0.8%) and plagioclase (50 ± 2.7%). The mineralogy of Em4, where CE-5 landed, and the other young basalts are shown in Extended Data Fig. 3. For both Em4 and the other young basalts, the olivine abundance is mostly less than around 10%, and high-Ca pyroxene is more abundant than low-Ca pyroxene. The young mare basalts cover a broader compositional area than Em4 (Extended Data Fig. 3), suggesting the presence of some diversity of basalts.

Age of the young mare basalts

The model age of all 30 young mare units was obtained through CSFD measurements with craters counted using an automatic method followed by careful manual checking³⁰. The new lunar chronology

function calibrated by the CE-5 basalts¹⁸ was used to derive the age of each unit. A map of the model age of the young mare basalts was then produced (Fig. 5).

For the young mare unit on which CE-5 landed (Em4 or U2), the model age is $1.95^{+0.14}_{-0.13}$ Ga, consistent with the isotopic ages of the samples (1,963 ± 57 Ma,¹³; 2,030 ± 4 Ma,¹⁴). The unit on which CE-3 (U28) landed has an age of $1.40^{+0.15}_{-0.14}$ Ga, younger than CE-5, both representing the deposits of the young Eratosthenian-aged mare volcanism.

Most of the young basalts have model ages older than 1.8 Ga (64.8% by area), including U1, U2, U4, U5, U6, U7, U8, U9, U10, U12, U15, U16, U20, U21, U22, U25, U27, U29 and U30 (Supplementary Table 2). U3 is the youngest mare unit ($1.47^{+0.18}_{-0.16}$ Ga) in northern Oceanus Procellarum, between the Aristarchus Plateau and Lichtenberg crater (Fig. 5). The mare basalts (U24, $1.36^{+0.18}_{-0.16}$ Ga; U26, $1.46^{+0.072}_{-0.068}$ Ga; U28, $1.40^{+0.15}_{-0.14}$ Ga) in northwestern Mare Imbrium are the youngest in the basin. The youngest unit among all young basalts in the PKT is located to the northeast of Kepler crater, with an age of $1.19^{+0.18}_{-0.16}$ Ga (U17). U10, on the south of Aristarchus Plateau (P60 in³), was previously thought to be the

youngest mare unit on the Moon. However, our results show that U10 has an age of $1.89^{+0.34}_{-0.29}$ Ga, older than a previous estimation ($1.2^{+0.32}_{-0.35}$ Ga³) and more consistent with the average age ($2.03^{+0.36}_{-0.32}$ Ga) proposed recently by Stadermann et al.³¹.

Discussion

Underrepresented evolved young volcanism

The composition of Apollo^{32,33}, CE-3 (ref. 27) and CE-5 (refs.13, 20, 21) basalts were summarized together (Extended Data Fig. 4). The CE-3 site has a CSFD model age of roughly 1.4 Ga. APXS data²⁷ shows that the CE-3 basalt is a low-TiO₂ (5.0%), low-Al₂O₃ (9.7%), low-K₂O (0.11%) mare basalt, with a low Mg# of 38. Olivine ($13.8 \pm 5.7\%$) and pyroxene ($51.9 \pm 2.1\%$) are two major mafic minerals within the CE-3 basalts. The CE-5 site has an isotopic age of 2.0 Ga^{13,14}. According to the returned samples, the CE-5 basalt is a low to intermediate-TiO₂ (5.0%), low-Al₂O₃ (10.8%), low-K₂O (0.19%) basalt²¹, with a low Mg# of 34. Olivine (8.5%) and pyroxene (40.1%) are two major mafic minerals (Fig. 2c).

The CE-3 and CE-5 sites are both located within the PKT, with similar age and composition. The pyroxene compositions from the CE-3 (ref. 27) and CE-5 (Fig. 2d) are also similar to each other. In addition, Apollo 12032,366-18 shares similarities with the CE-3 and CE-5 basalts. It is a type of low-TiO₂ (4.2%), high-Al₂O₃ (11.7%) and high-K₂O (0.25%) basalt, with a low Mg# of 40 (ref. 33). Apollo 12032,366-18 is thought to be delivered to the Apollo 12 site from northwestern Oceanus Procellarum, probably from a young mare region³³. Plotting major element contents together clearly shows that the CE-3, CE-5 and 12032,366-18 basalts are comparable to each other, and probably represent a type of basalt underrepresented in the Apollo catalogue. This underrepresented young basalt is enriched in Fe and depleted in Mg, with low Mg#, suggesting that they are the products of highly evolved volcanism²¹.

Young mare basalts in the PKT

The reinterpretation of young basalt mineralogy based on the CE-3 and CE-5 ground truth and the update of their ages using the new chronology function¹⁸ have provided new insights into the nature of young mare volcanism in the PKT.

We found that the olivine abundance of the young basalts (<10%) is significantly less than previously suggested^{5,6} (Fig. 4c), supported by the recent lunar mineral maps based on Kaguya Multiband Imager data³⁴. The broad 1 μm and weak 2 μm spectral features of the young basalts are likely to be due to the high-Ca clinopyroxene close to type A instead of abundant olivine, when abundant Fe²⁺ is sited at the M1 crystallographic site. The high abundance of olivine had been misinterpreted before for basaltic meteorites due to the presence of type A clinopyroxene³⁵.

The young basalts in Oceanus Procellarum and Mare Imbrium are slightly distinctive (Fig. 4 and Extended Data Fig. 2). The band I and II centre wavelengths of the young basalts in Oceanus Procellarum are longer than Mare Imbrium, and Oceanus Procellarum has a higher olivine but lower high-Ca pyroxene and low-Ca pyroxene abundances than Mare Imbrium (Fig. 4 and Extended Data Fig. 2), probably suggesting different eruption processes.

A map of model ages of all mare basalts in the PKT (Fig. 6a) was produced by combining the ages of the young basalts from this study and other basalts from Hiesinger et al.³. Most of the young basalts are located in the area surrounding the Aristarchus Plateau. The relative eruption flux was estimated according to the area of the basalts and their ages (Fig. 6d). In the PKT, the eruption flux decreased significantly after 3.5 Ga, reaching the lowest point around 2.5 Ga, before the second peak at around 2.0 Ga. Mare basalts with ages of around 2.0 Ga are widespread in the centre of the PKT (greenish polygon, Fig. 5) with an area of more than 330,000 km², including U2 where CE-5 landed. It indicates mare volcanism is still active at 2.0 Ga in the PKT and an additional heat source or mechanism may be needed at that time. The returned CE-5 basalts are providing crucial information to reveal potential heat source or mechanism.

When considering the composition and ages of the young basalts together (Fig. 6b,c), the younger basalts tend to have higher abundance of TiO₂, if U8, U9, U12, U16, U29 and U30 are excluded (grey points, Fig. 6b,c). The all these six units are older than 2.2 Ga and occur at the margins of the young basalts. We interpret this to mean that two different sources existed in the PKT: one is the source for lavas of the young basalts, with increasing TiO₂ abundance with time, and includes the CE-5 basalts; the second basalt source region is not on this trend. A similar distinction was observed by Kato et al.³⁶.

Young basalts, widespread in the PKT, are very high priority exploration and sampling targets because of their scientific significance for understanding late lunar thermal evolution⁹. However, CE-5 has returned 1,731 g of young basalts, more samples are required to better understand their generation, ascent and eruption of the entire population of young basalts. Two distinct young mare regions were identified within the PKT, that is, the basalts between Lichtenberg crater and the Aristarchus Plateau (U3) and those to the northeast of Kepler crater (U17). U3 has the highest TiO₂ ($11 \pm 1\%$) and olivine abundances ($13 \pm 0.8\%$, Fig. 4f). U17 has the youngest age ($1.19^{+0.18}_{-0.16}$ Ga) among mare basalts on the Moon. Both units should be listed as high priority sample-return targets for future explorations.

Methods

Mineralogy of the CE-5 sample CE5C0400

The CE-5 sample CE5C0400 (YJFM00403), weighing 200 mg, was used to determine the mineral abundance and composition at the CE-5 landing site. More information on this sample is described in the Lunar Sample Information Database (<https://moon.bao.ac.cn/moon-SampleMode/index.html>).

The lunar soil particles were analysed at the State Key Laboratory of Biogeology and Environmental Geology, China University of Geosciences, Wuhan, using the WITec α300R confocal Raman system equipped with the ParticleScout automated analysis tool. Small aliquots of the sample were dispersed on a carefully cleaned glass slide with ultrapure water and dried on a hot plate at 60 °C. Large area image stitching and focus stacking were performed with ×20 (numerical aperture (NA) of 0.50) or ×50 (NA 0.80) dark field objectives. Particles were automatically recognized from the images obtained on the basis of their brightness, which allows the reconstruction of particle distribution maps. For Raman analysis, particles with grain sizes between 1 and 45 μm and solidity greater than 0.85 were selected to exclude aggregates of multiple grains. Automatic focusing was applied during the Raman analysis of each particle to obtain a spectrum with the highest signal to noise ratio (SNR). A 532 nm laser was used with output laser power maintained between 3 and 5 mW. The integration time was set between 2 and 5 s with five to eight accumulations to obtain spectra with a fair SNR. Among the 12,404 analysed particles, 4,830 grains were identified using a customized spectral database of CE-5 minerals and then manually validated (Supplementary Data 2). The documented mineral phases include pyroxene, plagioclase, olivine, Fe oxides and minor or trace phases (for example, phosphate and quartz) (Fig. 2a). Modal abundances of these phases were calculated on the basis of the sum of the spherical equivalent volume ($VSE = \pi \times (d_{CE}^3/6)$), where d_{CE} refers to the circular equivalent diameter of the particles.

In addition, 612 larger grains were randomly picked, and their particle sizes were between 50 and 300 μm. The TIMA (3XGHM) system at the State Key Laboratory of Continental Dynamics, Northwest University, China, has obtained quantitative mineral abundances of these larger grains. The TIMA system comprises a TESCAN MIRA3 Schottky field emission scanning electron microscopy and nine detectors, including four high flux EDS detectors (EDAX Element 30) arranged at 90° intervals around the chamber. In this study, the dot mapping analysis mode has been used with X-ray counts set to 20,000, pixel spacing of back scattered electron (BSE) set to 1 μm and dot spacing of EDS set to 3 μm. The measurements have been conducted in a high

vacuum environment, with an acceleration voltage of 25 kV, electricity of 9 nA and a working distance of 15 mm. The electricity and BSE signals were calibrated by platinum Faraday cup and EDS signals by Mn standard. TIMA can automatically compare the measured BSE and EDS data of each different phase with the database and then distinguish their mineral phases (main phases, augite, glass, plagioclase, olivine and ilmenite; minor phases, quartz, K-glass, K-feldspar, apatite and so on) and compute mineral abundances. In total, the mineralogy of 612 grains has been determined (Fig. 2b), including 24% crystal fragment, 40% lithic fragment and 36% agglutinates.

The main element compositions of pyroxene and olivine were measured using a JEOL JXA-8230 EMPA at the State Key Laboratory of Geological Processes and Mineral Resources, China University of Geosciences, Wuhan, equipped with five wavelength-dispersive spectrometers. The samples were first coated with a thin conductive carbon film before analysis. Mineral analyses were conducted by using 15 kV accelerating voltage, 20 nA focused beam (1 µm diameter). The following standards were used with the ZAF (stopping power, back-scattering factor and X-ray production power, absorption and fluorescence) matrix correction: jadeite (Na), olivine (Si), diopside (Ca, Mg), sanidine (K), rutile (Ti), almandine garnet (Fe, Al), rhodonite (Mn), durango (F) and chromium oxide (Cr). The peak counting time was 10 s for Na, Mg, Al, Si, K, Ca, Fe, Cr and 20 s for Mn, Ti. The analysis uncertainty is better than 1% when the content of major elements is greater than 5%, and better than 5% when the content of major elements is 1–5%. The detection limit of Na, Si, Mg, Al, K, Mn, P, Ca, Ti, Fe and Cr are 103, 170, 106, 148, 75, 146, 118, 87, 233, 163 and 170 ppm, respectively.

In total, the compositions of 164 pyroxene grains and 47 olivine grains were measured from mineral and lithic fragments (Fig. 2de). Wo ($100 \times \text{molar Ca}/(\text{Mg} + \text{Fe} + \text{Ca})$), En ($100 \times \text{molar Mg}/(\text{Mg} + \text{Fe} + \text{Ca})$) and Fs ($100 \times \text{molar Fe}/(\text{Mg} + \text{Fe} + \text{Ca})$) numbers of pyroxene and Fo ($100 \times \text{molar Mg}/(\text{Mg} + \text{Fe})$) numbers of olivine were then determined on the basis of the EMPA results. The ideal site allocation of cations at T, M1 and M2 were calculated following the steps of Morimoto et al.²⁵: (1) sum T to 2.00 using Si^{4+} then Al^{3+} ; (2) sum M1 to 1.00 using any excess Al^{3+} , then add Ti^{4+} , Cr^{3+} , Ni^{2+} , Mg^{2+} , Fe^{2+} and Mn^{2+} until the sum is 1.00 and (3) sum M2 to 1.00 using any excess Mg^{2+} , Fe^{2+} and Mn^{2+} , then add Ca^{2+} , Na^+ and K^+ . If the sum of M2 is far from 1.00, then the EMPA data may be inaccurate.

Representativeness of the CE-5 samples to the Em4 unit

The CE-5 samples are interpreted to be representative of the regional geological unit (Em4) on which it landed, on the basis of comparing the compositional data obtained from orbit^{37,38} and from laboratorial analysis of the samples (TiO₂, 5.0% wt%; FeO, 22.5 wt%; Th, 4.72 ppm)²¹. Measured rare earth element contents of the CE-5 samples show that most of the pyroxene falls along the 1:2 line on a Ti/Al diagram and both pyroxene and plagioclase have similar rare earth element patterns, indicating a single basaltic lava flow at the CE-5 site²⁰. In addition, according to the investigation of impact craters adjacent to the CE-5 site, CE-5 landed on the ejecta blanket of Xu Guangqi crater³⁹, a crater that excavated down only into Em4, but not deep enough to excavate underlying older basalts. Therefore, the returned CE-5 samples are very likely to represent the Em4 unit.

Chang'e-3 VNIS

The VNIS is one of the main scientific payloads on the Yutu rover, and is based on two acousto-optic tunable filters¹⁵. It consisted of a VIS/NIR imaging spectrometer (450–950 nm), a short-wave infrared (SWIR) spectrometer (900–2,400 nm) and a calibration module. The VIS/NIR channel has a spectral resolution of 2–7 nm, with a SNR of >31 dB and the SWIR channel has a spectral resolution of 3–12 nm, with a SNR of >32 dB.

In this study, the reflectance of four in situ VNIS measurements were used, after dark-current subtraction, correction for the effect of temperature, radiometric calibration, geometric calibration²⁶, Sun–Moon distance correction and converting to reflectance⁴⁰.

The spectra obtained were then smoothed by a Savitzky–Golay filter (Supplementary Fig. 1), and their continuum was removed using the convex hull method (Fig. 3a).

The Chang'e-3 VNIS data are available through China's Lunar and Planetary Data Release System (<https://moon.bao.ac.cn/web/enmanager/home>).

Chang'e-5 LMS

The LMS is an acousto-optic tunable filter spectrometer onboard CE-5 (ref. 11). LMS has four measurement channels: visible (VIS, 480–950 nm), NIR (900–1,450 nm), SWIR (1,400–2,300 nm) and mid-wave infrared (2,200–3,200 nm). In all-band detection mode, LMS can obtain spectral images using the VIS channel and spectra using the three infrared channels. The VIS channel has a spectral resolution of 2.4–9.4 nm with a SNR of >34 dB, and the infrared channels have a spectral resolution of 7.6–24.9 nm with a SNR of >39 dB.

In this study, eight of the 11 in situ LMS measurements (Fig. 1b and Supplementary Fig. 2) in the detection mode were used. For the obtained 11 spectra, CE5-D04, CE5-D08, CE5-D09, CE5-D10, CE5-D12, CE5-D14, CE5-D15, CE5-D16 and CE5-D17 are from the lunar regolith; CE5-D06 and CE5-D11 are from Shigandang Rock (Fig. 1b). CE5-D04 and CE5-D12 were not used because of the splicing issues of VIS and NIR channels. CE5-D06 was not used because this spectrum may be contaminated by the light reflected from the robotic arm, according to the experiment team.

We started with level 2B irradiance data, which have been dark-current, flat-field, temperature, radiometric and geometric calibrated¹¹. The irradiance spectra have been converted to reflectance divided by the solar irradiance:

$$\frac{I}{F(\lambda_i)} = \frac{\pi I_s(\lambda_i)}{J(\lambda) S(\lambda) d\lambda}$$

where $J(\lambda)$ is the solar irradiance at 1 a.u. (astronomical unit), $S(\lambda)$ is the spectral response of the VNIS sensor. $I_s(\lambda_i)$ is the radiance at wavelength λ_i .

The spectra obtained were then smoothed by a Savitzky–Golay filter (Supplementary Fig. 1), and their continuum was removed using the convex hull method (Fig. 3b).

The Chang'e-5 LMS data are available through China's Lunar and Planetary Data Release System (<https://moon.bao.ac.cn/web/enmanager/home>).

Chandrayaan-1 M³

The M³ is a push-broom imaging spectrometer onboard Chandrayaan-1 (ref. 17) that operated from the VIS into the NIR (0.43–3.0 µm). The thermally corrected optical period 2C (OP2C) data²⁸ have been used to extract the spectra of small fresh craters. This dataset has a resolution of 280 m per pixel²⁸ and a full coverage of the young mare basalts within the PKT.

The spectra of 200 small fresh craters within Em4 and 1,741 small fresh craters within young mare region have been extracted from the M³ data. The extracted M³ spectra were then smoothed using a Savitzky–Golay filter, and their continuum was removed using the convex hull method before further analysis, the same method as used for the VNIS and LMS data. In addition, the band I and band II centre positions of each M³ spectra were determined by searching the local minima between 800 and 1,300 nm, and 1,700 and 2,300 nm, respectively.

Lookup table

A lookup table technique was used to obtain the absolute mineral abundance of the small fresh craters within the young mare region. The technique is based on the synthesized spectra calculated using the Hapke radiative transfer model⁴¹. We follow the routine of Sun et al.¹⁶ which considers the variable Mg# ($100 \times \text{molar Mg}/(\text{Mg} + \text{Fe})$) of lunar surface materials. The model uncertainties are described in

detail by Sun et al.¹⁶. According to the sensitivity test¹⁶, the lookup table technique has an accuracy of 0.8% for olivine, 1.1% for low-Ca pyroxene, 1.0% for high-Ca pyroxene and 2.7% for plagioclase. In our modelling, low-Ca pyroxene includes pigeonite, which belongs to clinopyroxene.

The lookup table technique set up is briefly summarized here. We consider four major minerals in our lookup table, with high-Ca pyroxene varying from 0 to 50%, low-Ca pyroxene varying from 0 to 30% and olivine varying 0–30% at intervals of 2%, and plagioclase varying from 10 to 60% at intervals of 3%. SMFe was set between 0 and 0.05 at intervals of 0.01, and Mg# was set between 15 and 60 at intervals of five to match the evolved nature of young lunar volcanism. In total, a spectral library of 74,970 modelled spectra was constructed.

To search the best fit spectra from the lookup table to the investigated M³ spectra, the criterion used by Sun et al.¹⁶ was used here ($CR = 0.8 \times r.m.s. + 0.2 \times (1 - |R|)$), where the best fit spectra have the smallest criterion value (CR). The FeO content of the M³ spectra was calculated by the method of Kumar et al.⁴², with an optimized origin at (0.08, 1.18). In searching, the difference in FeO between the M³ spectra and the synthesized spectra was limited within 2 wt.%.

Using this method, the absolute mineral abundance of 200 small fresh craters within Em4 and 1,741 small fresh craters within the young mare region were determined. The Kriging method was used to interpolate the absolute mineral abundance of 200 spectra for Em4 and 1,741 spectra for the young mare region (Fig. 4 and Extended Data Fig. 2), to understand the spatial distribution of key minerals in the young mare region.

We have chosen four examples of M³ spectra and their best fit synthesized spectra (Supplementary Fig. 3) for comparison and test the method. Em4-16 and Em4-46 represent the spectra extracted from Em4 with no olivine and most abundant olivine. U3-4 and U22-10 represent the spectra of the U3 and U22 units with no and most abundant olivine. Although the 1 μm feature is broad, it does not require the presence of significant olivine. The concentration of high-Ca clinopyroxene close to type A can also account for the broad 1 and weak 2 μm features⁴³. Em4-19 and Em4-46 (Supplementary Fig. 3) only have olivine abundances of 0 ± 0.8 and $10 \pm 0.8\%$, respectively. However, both have a broad 1 μm and a weak 2 μm absorption. U3-4, between the Aristarchus Plateau and Lichtenberg crater (Fig. 1) with highest olivine abundance documented by Staid et al.⁵ and Zhang et al.⁶, has a distinct broad 1 μm feature (Supplementary Fig. 3c); however, it only contains $16 \pm 0.8\%$ olivine, far smaller than previous estimates^{5,6,8}. Furthermore, U22-10, between Euler and Lambert craters (Fig. 1), has a 1 μm feature that is not narrow and a 2 μm feature that is deeper than the olivine-rich rocks (Supplementary Fig. 3d), suggesting almost no olivine in this unit.

CSFD measurements

The model ages of the 30 mapped young mare units were obtained through CSFD measurements. The geological boundaries were delineated on the basis of the LROC WAC albedo and Clementine UV-vis false colour maps on the basis of previous works^{3,6,44}.

Impact craters were counted using an automatic method³⁰ based on Kaguya Terrain Camera data (10 m per pixel). In total, 415,099 craters larger than 280 m were identified in the young mare basalt region. Crater counting areas were selected for each mare unit (pink polygon, Extended Data Fig. 1a,b) on the basis of LROC WAC albedo and Clementine TiO₂ abundance maps to avoid areas contaminated by extensive secondary craters or deformed by wrinkle ridges. For each crater counting area, careful manual checking of the automatic counting results was conducted to remove those misidentified craters or secondary craters. After that, the final recognized craters of each unit were exported to Craterstats⁴⁵ to derive the model ages, using the production function of Neukum⁴⁶ and the chronology function of Yue et al.¹⁸. The new lunar chronology function calibrated through the age (2.0 Ga) of the CE-5 basalts^{13,14,18} for the less constrained range of the function between

1.0 and 3.0 Ga⁹ is significant to update the ages of the young basalts because all of their ages are within this range³.

Data availability

CE-3 VIS-NIR Spectrometer data and CE-5 LMS data are available from China's Lunar and Planetary Data Release System (<https://moon.bao.ac.cn/ce5web/moonGisMap.search>) and also the Supplementary Tables 1 and 2 of this paper. CE-5 sample CE5C0400 (YJFM00403) was obtained by application from CNSA, according to the Notice of CNSA on the Distribution of Procedures for Requesting Lunar Samples (<http://www.cnsa.gov.cn/english/n6465645/n6465648/c6811126/content.html>). The NASA Reflectance Experiment Lab (RELAB) data are from the PDS Geoscience Node Spectral Library (<https://pds-geosciences.wustl.edu/spectrallibrary/default.htm>). Thermally corrected M³ data are from S. Li. Experiments were conducted in the State Key Laboratory of Geological Processes and Mineral Resources and the State Key Laboratory of Biogeology and Environmental Geology, China University of Geosciences, Wuhan, and State Key Laboratory of Continental Dynamics, Department of Geology, Northwest University.

References

1. Staid, M. I. & Pieters, C. M. Mineralogy of the last lunar basalts: results from Clementine. *J. Geophys. Res. Planets* **106**, 27887–27900 (2001).
2. Jolliff, B. L., Gillis, J. J., Haskin, L. A., Korotev, R. L. & Wieczorek, M. A. Major lunar crustal terranes: surface expressions and crust-mantle origins. *J. Geophys. Res. Planets* **105**, 4197–4216 (2000).
3. Hiesinger, H., Head, J. W., Wolf, U., Jaumann, R. & Neukum, G. Ages and stratigraphy of lunar mare basalts: a synthesis. *Spec. Pap. Geol. Soc. Am.* **477**, 1–51 (2011).
4. Pieters, C. M. et al. Late high-titanium basalts of the Western Maria: geology of the Flamsteed region of Oceanus Procellarum. *J. Geophys. Res. Solid Earth* **85**, 3913–3938 (1980).
5. Staid, M. I. et al. The mineralogy of late stage lunar volcanism as observed by the Moon Mineralogy Mapper on Chandrayaan-1. *J. Geophys. Res. Planets* <https://doi.org/10.1029/2010JE003735> (2011).
6. Zhang, X. et al. Mineralogical variation of the late stage mare basalts. *J. Geophys. Res. Planets* **121**, 2063–2080 (2016).
7. Varatharajan, I., Srivastava, N. & Murty, S. V. S. Mineralogy of young lunar mare basalts: assessment of temporal and spatial heterogeneity using M3 data from Chandrayaan-1. *Icarus* **236**, 56–71 (2014).
8. Lucey, P. G. Mineral maps of the Moon. *Geophys. Res. Lett.* <https://doi.org/10.1029/2003GL019406> (2004).
9. Tartèse, R. et al. Constraining the evolutionary history of the Moon and the inner Solar System: a case for new returned lunar samples. *Space Sci. Rev.* **215**, 54 (2019).
10. Zhao, J. et al. Geologic characteristics of the Chang'E-3 exploration region. *Sci. China Phys. Mech. Astron* **57**, 569–576 (2014).
11. Zhou, C. et al. Scientific objectives and payloads of the lunar sample return mission—Chang'E-5. *Adv. Space Res.* **69**, 823–836 (2022).
12. Qian, Y. et al. Geology and scientific significance of the Rümker Region in Northern Oceanus Procellarum: China's Chang'E-5 landing region. *J. Geophys. Res. Planets* **123**, 1407–1430 (2018).
13. Che, X. et al. Age and composition of young basalts on the Moon, measured from samples returned by Chang'e-5. *Science* **374**, 887–890 (2021).
14. Li, Q.-L. et al. Two-billion-year-old volcanism on the Moon from Chang'e-5 basalts. *Nature* **600**, 54–58 (2021).
15. Li, C. et al. The Chang'e 3 mission overview. *Space Sci. Rev.* **190**, 85–101 (2015).

16. Sun, L. & Lucey, P. G. Unmixing mineral abundance and Mg# with radiative transfer theory: modeling and applications. *J. Geophys. Res. Planets* **126**, e2020JE006691 (2021).
17. Pieters, C. M. et al. The Moon Mineralogy Mapper (M3) on Chandrayaan-1. *Curr. Sci.* **96**, 500–505 (2009).
18. Yue, Z. et al. Updated lunar cratering chronology model with the radiometric age of Chang'e-5 samples. *Nat. Astron.* **6**, 541–545 (2022).
19. van der Bogert, C. H. & Hiesinger, H. Which samples are needed for improved calibration of the lunar cratering chronology? In *Proc. 51st Lunar and Planetary Science Conference Abstract 2088* (Lunar and Planetary Institute, 2020).
20. Tian, H.-C. et al. Non-KREEP origin for Chang'e-5 basalts in the Procellarum KREEP Terrane. *Nature* **600**, 59–63 (2021).
21. Li, C. et al. Characteristics of the lunar samples returned by the Chang'E-5 mission. *Natl Sci. Rev.* **9**, nwab188 (2022).
22. He, Q. et al. Detailed petrogenesis of the unsampled Oceanus Procellarum: the case of the Chang'e-5 mare basalts. *Icarus* **383**, 115082 (2022).
23. Adams, J. B. in *Infrared and Raman Spectroscopy of Lunar and Terrestrial Minerals* (ed. Karr, C. B.) 91–116 (Academic Press, 1975).
24. Klima, R. L., Dyar, M. D. & Pieters, C. M. Near-infrared spectra of clinopyroxenes: effects of calcium content and crystal structure. *Meteorit. Planet. Sci.* **46**, 379–395 (2011).
25. Morimoto, N. Nomenclature of pyroxenes. *Mineral. Petrol.* **39**, 55–76 (1988).
26. Liu, B. et al. Data processing and preliminary results of the Chang'e-3 VIS/NIR imaging spectrometer in-situ analysis. *Res. Astron. Astrophys.* **14**, 1578–1594 (2014).
27. Ling, Z. et al. Correlated compositional and mineralogical investigations at the Chang'e-3 landing site. *Nat. Commun.* **6**, 8880 (2015).
28. Li, S. & Milliken, R. E. An empirical thermal correction model for Moon Mineralogy Mapper data constrained by laboratory spectra and Diviner temperatures. *J. Geophys. Res. Planets* **121**, 2081–2107 (2016).
29. Qian, Y., Xiao, L., Head, J. W. & Wilson, L. The long sinuous Rille system in Northern Oceanus Procellarum and its relation to the Chang'e-5 returned samples. *Geophys. Res. Lett.* **48**, e2021GL092663 (2021).
30. Wang, Y. & Wu, B. Active machine learning approach for crater detection from planetary imagery and digital elevation models. *IEEE Trans. Geosci. Remote Sensing* **57**, 5777–5789 (2019).
31. Stadermann, A. C. et al. The age of lunar mare basalts south of the Aristarchus Plateau and effects of secondary craters formed by the Aristarchus event. *Icarus* **309**, 45–60 (2018).
32. Wieczorek, M. A. et al. The constitution and structure of the lunar interior. *Rev. Mineral. Geochem.* **60**, 221–364 (2006).
33. Stadermann, A. C., Jolliff, B. L., Krawczynski, M. J., Hamilton, C. W. & Barnes, J. J. Analysis and experimental investigation of Apollo sample 12032,366-18, a chemically evolved basalt from the Moon. *Meteorit. Planet. Sci.* **57**, 794–816 (2022).
34. Lemelin, M. et al. The compositions of the lunar crust and upper mantle: Spectral analysis of the inner rings of lunar impact basins. *Planet. Space Sci.* **165**, 230–243 (2019).
35. Schade, U., Wäsch, R. & Moroz, L. Near-infrared reflectance spectroscopy of Ca-rich clinopyroxenes and prospects for remote spectral characterization of planetary surfaces. *Icarus* **168**, 80–92 (2004).
36. Kato, S. et al. Magma source transition of lunar mare volcanism at 2.3 Ga. *Meteorit. Planet. Sci.* **52**, 1899–1915 (2017).
37. Qian, Y. et al. Young lunar mare basalts in the Chang'e-5 sample return region, northern Oceanus Procellarum. *Earth Planet. Sci. Lett.* **555**, 116702 (2021).
38. Qian, Y. et al. China's Chang'e-5 landing site: geology, stratigraphy, and provenance of materials. *Earth Planet. Sci. Lett.* **561**, 116855 (2021).
39. Qian, Y. et al. Copernican-aged (<200Ma) impact ejecta at the Chang'e-5 landing site: statistical evidence from crater morphology, morphometry, and degradation mode. *Geophys. Res. Lett.* **48**, e2021GL095341 (2021).
40. Wu, Y., Wang, Z., Cai, W. & Lu, Y. The absolute reflectance and new calibration site of the Moon. *Astron. J.* **155**, 213 (2018).
41. Hapke, B. *Theory of Reflectance and Emittance Spectroscopy* (Cambridge Univ. Press, 2012).
42. Ajith Kumar, P. & Kumar, S. Estimation of optical maturity parameter for lunar soil characterization using Moon Mineralogy Mapper (M3). *Adv. Space Res.* **53**, 1694–1719 (2014).
43. Cloutis, E. A. & Gaffey, M. J. Pyroxene spectroscopy revisited: spectral-compositional correlations and relationship to geothermometry. *J. Geophys. Res. Planets* **96**, 22809–22826 (1991).
44. Chen, Y. et al. The thickness and volume of young basalts within Mare Imbrium. *J. Geophys. Res. Planets* **123**, 630–645 (2018).
45. Michael, G. G. Planetary surface dating from crater size–frequency distribution measurements: multiple resurfacing episodes and differential isochron fitting. *Icarus* **226**, 885–890 (2013).
46. Neukum, G. *Meteorite Bombardment and Dating of Planetary Surfaces* (Univ. Munich, 1983).

Acknowledgements

We thank the China National Space Administration for organizing and implementing the CE-3 and CE-5 missions and providing access to the sample and data. We thank S. Li for sharing with us the thermally corrected M³ data and Y. Wu for discussing the CE-3 VNIS data. This research is funded by the National Key R&D Programme of China (grant no. 2020YFE0202100), the Pre-Research Project on Civil Aerospace Technologies (grant nos. D020101, D020205) and the National Natural Science Foundation of China (grant nos. 41830214, 42172337). Y.Q. is funded by the China Scholarship Council grant no. 201906410015. J.M. and B.Y. were supported by the Hong Kong Research Grants Council Research Impact Fund Project no. R5043-19.

Author contributions

Y.Q., L.X., Z.W., Z.S. and Q.H. designed this research. Z.W., Q.H., X.W., K.Z., Z.H. and Z.S. applied the CE-5 samples from CNSA. Y.Q., L.S., J.M., B.Y. and S.Z. conducted spectral analysis. Z.S., K.C. and M.D. collected and analysed Raman data. Q.H., Y.L. and F.P. collected and analysed electron probe data. Z.W., Y.L. and W.S. collected and analysed TIMA data. Y.W. and B.W. detected impact craters. Y.Q., Z.S., Q.H., L.X., Z.W., J.W.H., L.S., Y.W., B.W., X.W., B.L., K.C., Y.L., M.D., W.S., F.P., J.M., B.Y., Jiawei Z., S.Z., J.H., Jiannan Z., J.W., K.Z. and Z.H. wrote the manuscript. Y.Q., Z.S., Q.H. and Y.L. produced figures. All authors reviewed the manuscript.

Competing interests

The authors declare no competing interests.

Additional information

Extended data is available for this paper at <https://doi.org/10.1038/s41550-022-01862-1>.

Supplementary information The online version contains supplementary material available at <https://doi.org/10.1038/s41550-022-01862-1>.

Correspondence and requests for materials should be addressed to Long Xiao or Zaicong Wang.

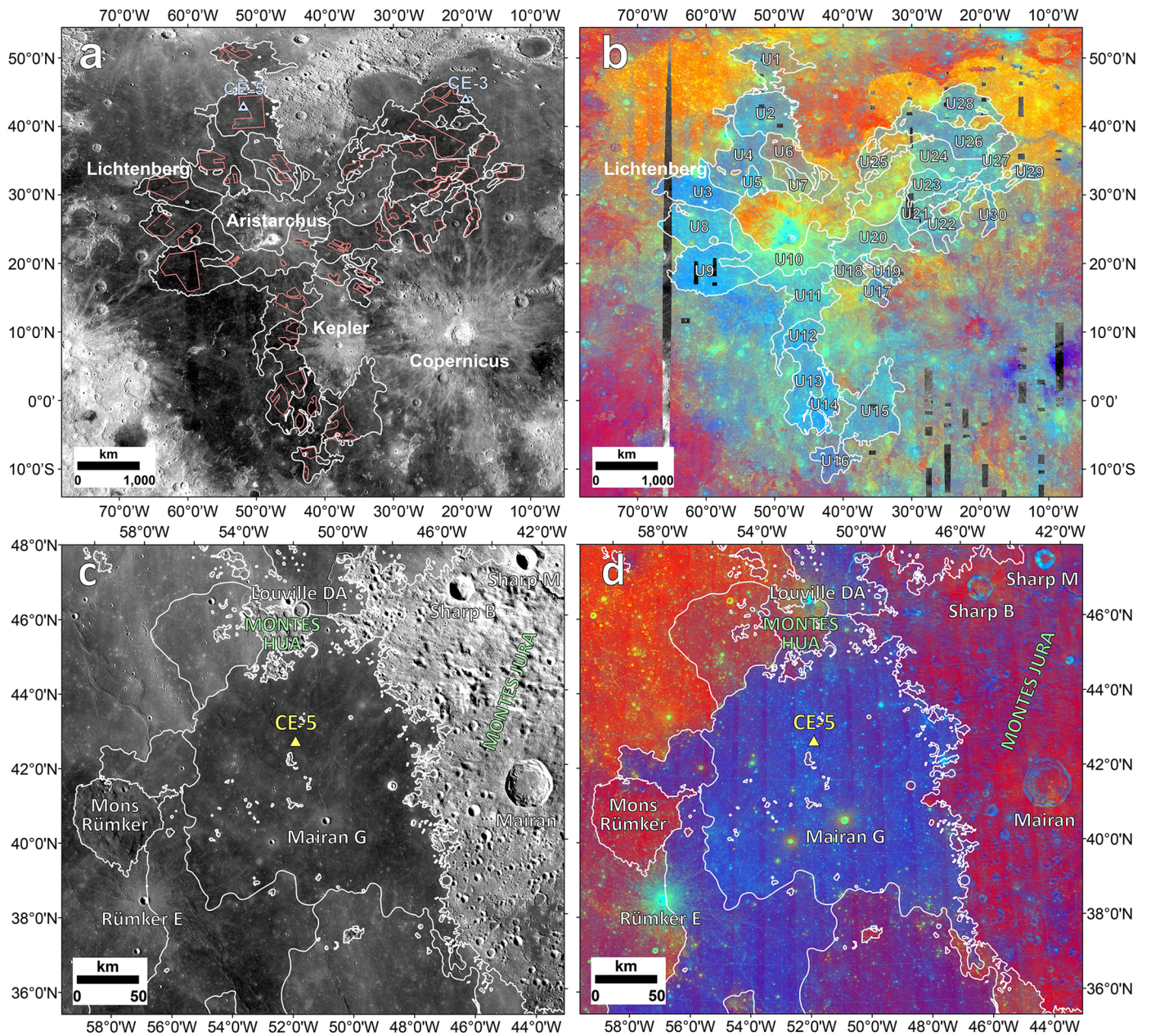
Peer review information *Nature Astronomy* thanks Joshua Snape, Katherine Joy and the other, anonymous, reviewer(s) for their contribution to the peer review of this work.

Reprints and permissions information is available at www.nature.com/reprints.

Publisher's note Springer Nature remains neutral with regard to jurisdictional claims in published maps and institutional affiliations.

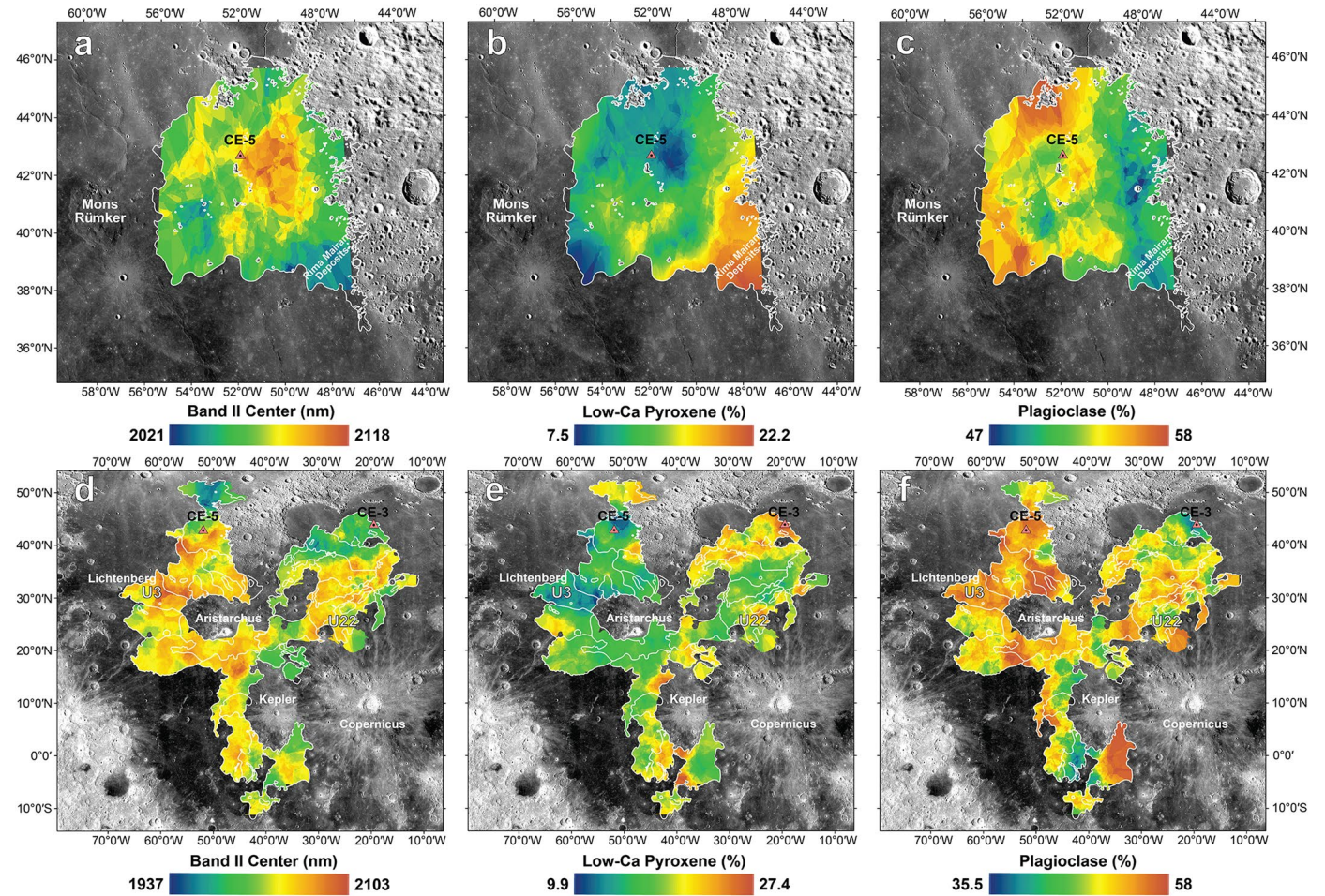
Springer Nature or its licensor (e.g. a society or other partner) holds exclusive rights to this article under a publishing agreement with the author(s) or other rightsholder(s); author self-archiving of the accepted manuscript version of this article is solely governed by the terms of such publishing agreement and applicable law.

© The Author(s), under exclusive licence to Springer Nature Limited 2023

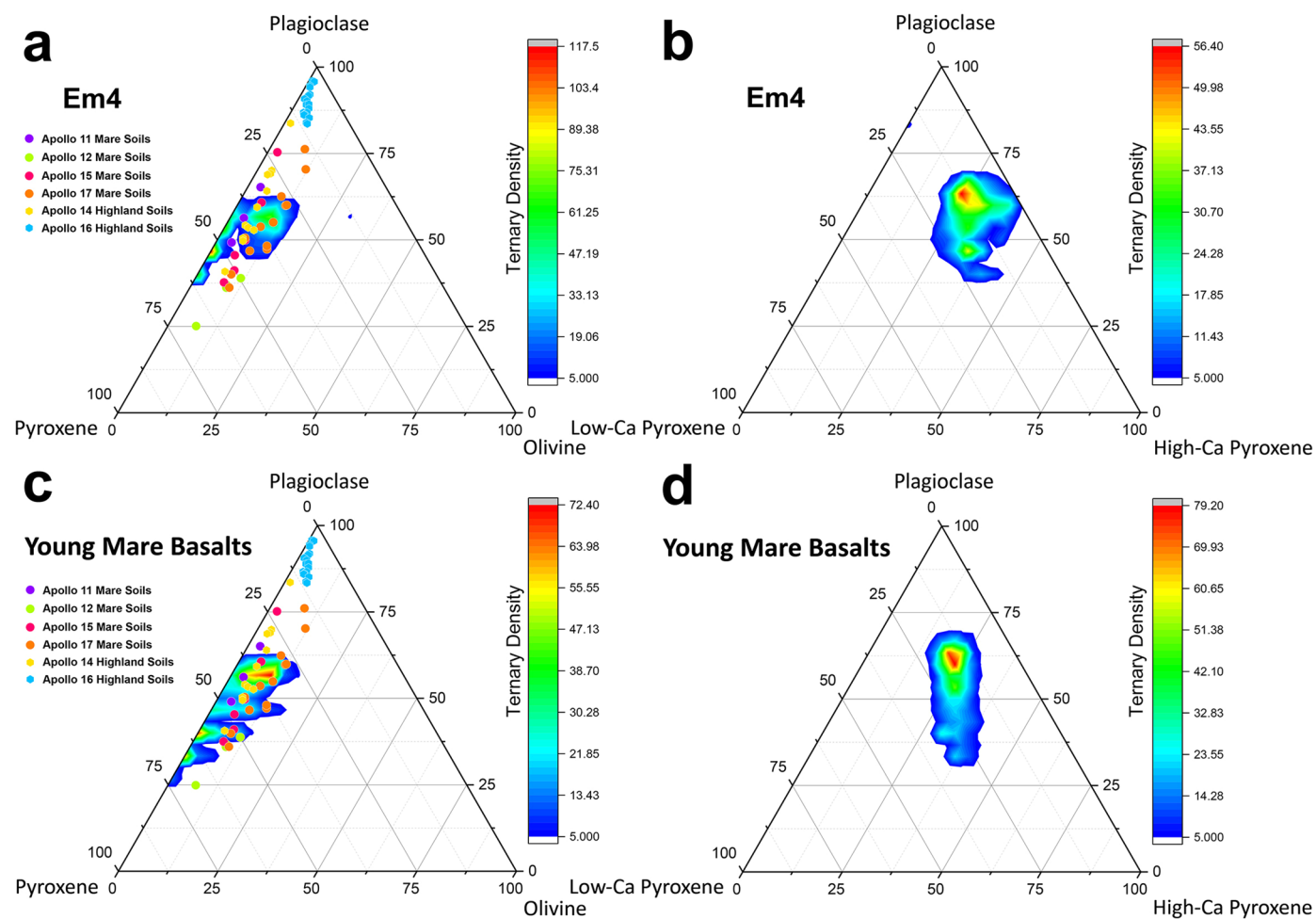


Extended Data Fig. 1 | Boundary of the young mare basalts. (a) Geological units of the young mare basalts (white lines). The pink polygon indicates the crater counting areas. The basemap is a LROC WAC image (NASA/GSFC/ASU). (b) Clementine UVVIS false color map of the young mare basalts. (c) LROC WAC

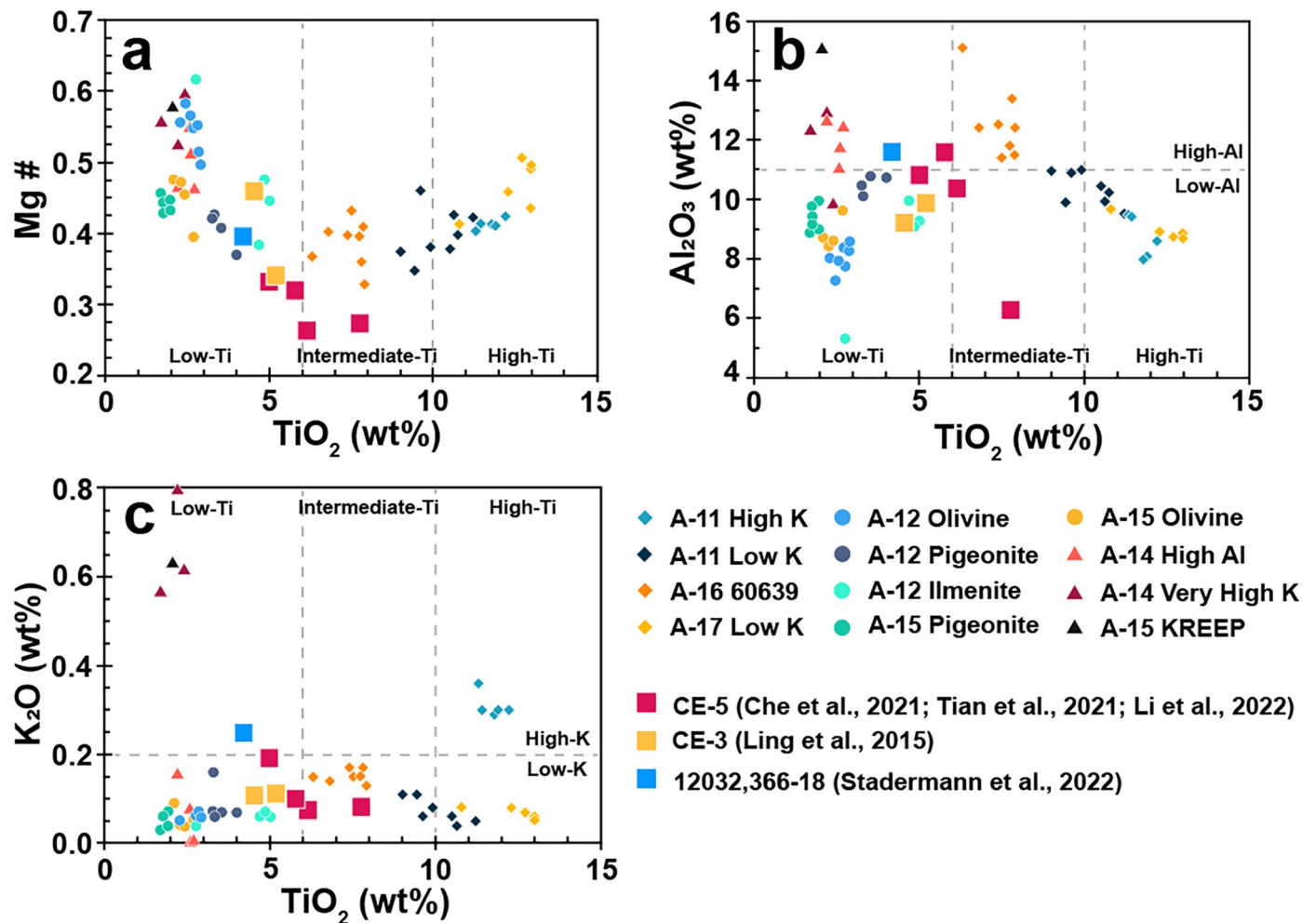
image of northern Oceanus Procellarum (NASA/GSFC/ASU). (d) Kaguya MI color composite of northern Oceanus Procellarum. The yellow triangle represents the CE-5 landing site. The white lines denote the geological boundaries.



Extended Data Fig. 2 | Mineralogy of Em4 and the young mare basalts. (a-c) Band II center position, low-Ca pyroxene abundance, and plagioclase abundance of Em4. (d-f) Band II center position, low-Ca pyroxene abundance, and plagioclase abundance of the young mare basalts. CE-5 landed on the Em4 unit. The basemap is a LROC WAC image (NASA/GSFC/ASU).



Extended Data Fig. 3 | Mineralogy of Em4 and young mare basalts. (a, b) Mineralogy of the Em4 unit. (c, d) Mineralogy of the young mare basalts. The olivine abundance is mostly smaller than 10% and high-Ca pyroxene is richer than low-Ca pyroxene.



Extended Data Fig. 4 | Compositions of the Apollo and Chang'e mare basalts. CE-3, CE-5, and A-12/12032, 366-18 represent a type of underrepresented young mare basalt in the Apollo collections. A-11 represent Apollo 11 and so on. This figure is modified from Che et al.¹³.